Sedimentary Geology 484-485 (2025) 106903

Contents lists available at ScienceDirect

Sedimentary Geology

journal homepage: www.elsevier.com/locate/sedgeo

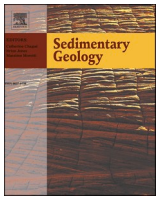

Quantitative reconstruction of paleowind strength based on ancient marine longshore bars: A case study of the Pinghu Formation in Pingbei slope zone, Xihu Sag

Jinlin Chen [a,b], Junhui Wang [a,b,*], Guofeng Yin [c], Yang Wu [a,b], Zhengming Dai [a,b], Yonglin Li [a,b], Jinhao Ma [a,b], Zaixing Jiang [d], Jie Xu [e]

[a] State Key Laboratory of Petroleum Resources and Engineering, China University of Petroleum (Beijing), Beijing 102249, China
[b] College of Geosciences, China University of Petroleum (Beijing), Beijing 102249, China
[c] SINOPEC Shanghai Offshore Oil & Gas Company, Shanghai 200120, China
[d] School of Energy Resources, China University of Geosciences (Beijing), Beijing 100083, China
[e] School of Ocean Sciences, China University of Geosciences (Beijing), Beijing 100083, China

ARTICLE INFO

Editor: Dr. Giorgio Basilici

Keywords:
Paleowind
Paleowave
Longshore bar
Breaker zone
Xihu Sag

ABSTRACT

Paleowind is an important paleoclimate parameter, but its study has been limited due to the lack of research methods. Recently, some researchers have proposed a method combining wind fields, waves, and the scale of ancient bar sand bodies to indirectly reconstruct paleowind. However, this method can only be used in lacustrine environments since in existing reconstruction methods, the fetch—a necessary parameter approximating the distance that wind blows—is difficult to obtain in marine environments. This study introduces the concept of "fully developed waves", eliminating the need of fetch, which improves the current method of reconstructing paleowind using bars and extends its application to marine environments. The method is easy to operate and it only needs two parameters: the thickness of longshore bars and the seabed slope. This study further focuses on the bars of the Pinghu Formation in the Pingbei slope zone of the Xihu Sag within the East China Sea Shelf Basin. Using the proposed method, the paleowind variations during the depositional period (37.2–35.5 Ma) were reconstructed. The results show that the Xihu Sag was primarily influenced by easterly winds during this time, with wind speeds ranging from 8.76 to 19.71 m/s. This method removes the limitation of using bars for quantitative paleowind reconstruction exclusively in lacustrine settings, thereby enhancing its application potential and contributing to providing more data for paleoclimate reconstruction.

1. Introduction

Wind fields are the result of atmospheric circulation, influencing temperature variations and precipitation patterns. Research on wind fields is a critical topic in global climate change studies (Young et al., 2011; Young and Ribal, 2019; Kifumbi et al., 2023; Chen et al., 2024). Currently, studies on paleowind fields are relatively scarce, primarily due to a lack of research methods. Most existing studies on paleowind fields focus on qualitative analysis, such as winds' directions or relative strength (Lagroix and Banerjee, 2002; Troiani et al., 2011; Ge et al., 2014; Xue et al., 2021; Mau et al., 2022; Hu et al., 2023; Liu et al., 2024; Xie et al., 2024). This is because studying paleowind fields requires the use of sedimentary records associated with wind activities, which are hard to gain.

The influence of wind on sediments can be categorized into two types: direct and indirect effects. Direct effects refer to the transportation and modification of sediment particles directly by wind. By establishing a relationship between the particle size of aeolian sediments and the wind field's transport capacity, paleowind can be reconstructed using sedimentary dynamics principles (Davidson-Arnott and Bauer, 2009; Eastwood et al., 2012; Wang et al., 2018a). The sedimentary record used in these methods are deposited under the directly influence of wind, making it highly correlated with the wind field and relatively reliable (Bauer et al., 2009; Favaro et al., 2024; Liu et al., 2024). However, aeolian sediments are relatively difficult to preserve in the sedimentary record, so these applications are limited.

* Corresponding author at: State Key Laboratory of Petroleum Resources and Engineering, China University of Petroleum (Beijing), Beijing 102249, China.
E-mail address: wangjunhui@cup.edu.cn (J. Wang).

https://doi.org/10.1016/j.sedgeo.2025.106903
Received 20 February 2025; Received in revised form 21 May 2025; Accepted 28 May 2025
Available online 31 May 2025

In addition to acting directly on sediments, wind can also influence sediment transport and modification indirectly by driving water bodies in lakes or oceans to generate waves (Chai et al., 2024; Hu et al., 2024; Li et al., 2024a). Compared to aeolian deposits, wave deposits are more common. As waves propagate toward the shore, they can transport unconsolidated sediments on the sea (or lake) floor and deposit large amounts of sediment in the coastal zone, forming beaches and bars (Airy, 1845; Le Roux, 2015; Wang et al., 2018b). During this process, bars would record the information about the direction and magnitude of ancient waves, making it feasible to reconstruct paleowind indirectly after restoring ancient wave characteristics (Adams, 2003; Jiang et al., 2018; Wang et al., 2018b).

Based on the research framework described above, Jiang et al. (2018) proposed a method for reconstructing paleowind speed using longshore bars in ancient lakes. Here is a brief introduction to this method:

This method involves collecting three parameters for a single-phase longshore bar: its thickness (t), the seabed slope (α), and the paleofetch of wind (F). The thicknesses of longshore bars are measured from rock cores or well-log data and the seabed slope is obtained by paleotopograpgy reconstruction based on basin analyses. When t and α are known, the water depth of breaking waves (d_b) can be calculated. And then, water depth of breaking waves (d_b) can be converted into breaking wave height (H_b) by reading the graph of Goda (1970).

Besides, in this method, operator also have to identify the shoreline of the ancient lake for measuring the distance between longshore bars and the edge of basin, which is used to estimate paleofetch (F). When breaking wave height (H_b), which is assumed as the maximum height of the waves, and paleofetch (F) are known, the speed of wind can be calculated in this fetch-limited conditions.

In this method, paleofetch is a critical parameter, and errors in it significantly impact the accuracy of wind speed reconstruction, which makes the method difficult to use. Theoretically, the application of this method is limited to lacustrine basins, since the method approximates fetch as the distance from the location of longshore bar development upwind to the edge of the ancient lake. For marine basins, it is impractical to measure the entire width of an ancient ocean to determine paleofetch.

Therefore, reconstructing paleowind in marine basins requires addressing the challenge of paleofetch being unobtainable. To resolve this issue, this study proposes a new method for reconstructing paleowind by using longshore bars without the need for paleofetch. The method is applied to the Pingbei slope zone of the Xihu Sag in the East China Sea Shelf Basin, utilizing longshore bar deposits developed during the Pinghu Formation to reconstruct paleowind for that period.

2. Principles and methodology

2.1. Sedimentary characteristics of longshore bar

Longshore bars are a type of bar deposit formed in the breaker zone of nearshore environments. Its sedimentation processes are directly

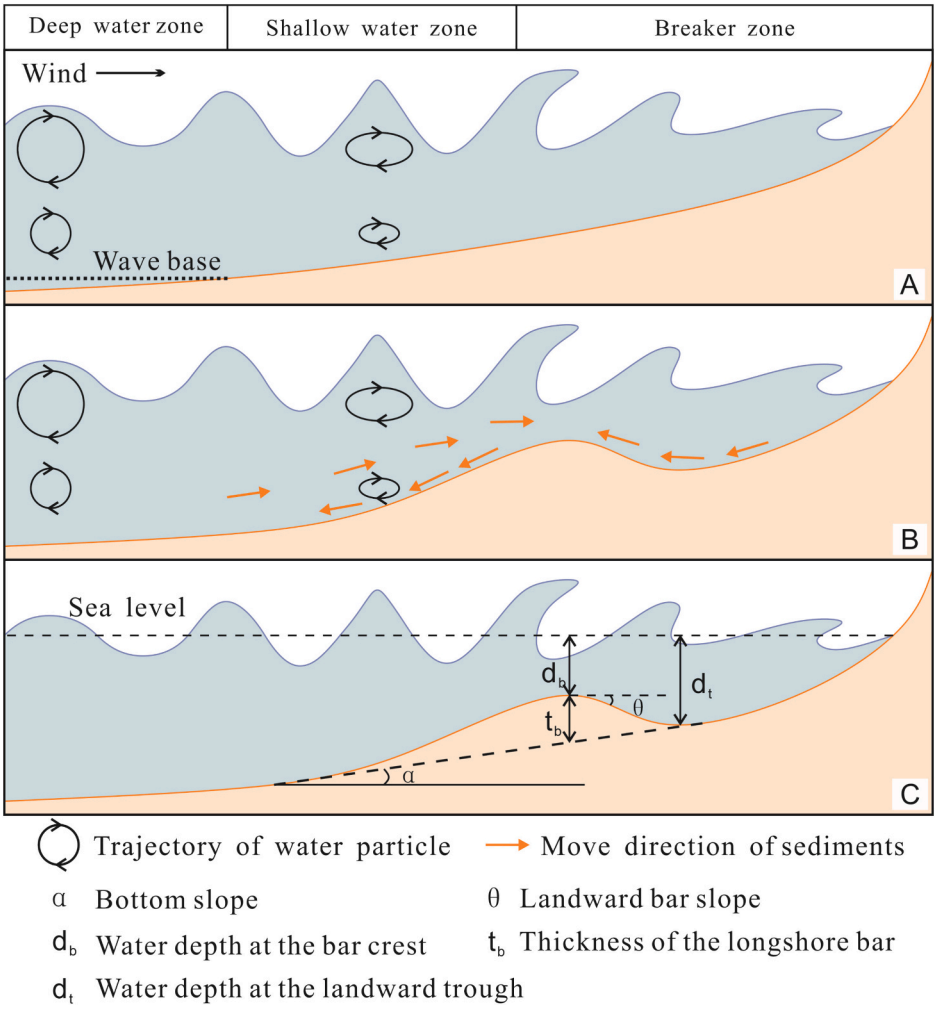

Fig. 1. Equilibrium model diagram of longshore bar (modified from Davidson-Arnott, 2011; Wang et al., 2021). (A) Movement trajectory of water particle blew by wind. (B) Fully established longshore bar that has reached an equilibrium state. (C) Diagram of each parameter.

controlled by breaking waves (Jiang et al., 2018). When waves propagate from deep water to the shore, the water particles interact with the seabed, causing waves deformation and their break down (Fig. 1A). The energy of waves accumulation during the deformation and release when they break. The area where the waves break is called breaking zone. It is the first major energy dissipation zone of wave propagation. In this region, not only are large amounts of sediment carried by waves deposited, but also loose clastic sediments in the area are reshaped by wave activities (Davidson-Arnott, 2011). These processes work together to form longshore bars. In addition to the dominant shoreward propagation of waves, the breaker zone also features offshore-directed undertows (Biausque et al., 2020). This bottom current can transport sediment toward deeper water (Fig. 1B). Through repeated wave-driven transport, sediments gradually accumulate in the breaker zone, leading to the formation of longshore bars.

The self-organizational model is one of the most widely accepted explanations for the formation of longshore bars (Dyhr-Nielsen and Sørensen, 1970). It posits that, when longshore bars form in the breaker zone, sediments transported shoreward by dominant wave and sediment transported seaward by undertow reach an equilibrium state. In this equilibrium, the sediment transport rates in both directions are equal over a given period. Under ideal conditions, when a longshore bar achieves this balance with the waves, the bar's position, thickness, and water depth above its crest will remain constant (Coco and Murray, 2007).

The parameters mentioned above are determined by the waves that create the longshore bar. Larger waves break in deeper water, resulting in a larger bar, and vice versa (Ruessink and Kroon, 1994; Pruszak et al., 1997). As a wave increases in size, the longshore bar migrates seaward into deeper water, leading to an increase in water depth above the bar crest and in the trough behind the bar. Conversely, if wave intensity is weaker, the longshore bar would migrate shoreward, and its equilibrium size becomes smaller.

2.2. Relationship between longshore bars and breaking waves

According to the self-organizational model of longshore bars, although waves of different sizes produce longshore bars of varying scales, the morphology of these bars remains consistent (Wang et al., 2021). Due to the seabed slope, loose sediments slope toward the basin, which creates asymmetry in the cross-shore profile of the longshore bar (Fig. 1B). The offshore side of the bar tends to be relatively gentle, while the nearshore side is steeper (Dyhr-Nielsen and Sørensen, 1970; Davidson-Arnott, 2011). On the other hand, the morphology of the bar is generally uniform in the alongshore direction. As a result, descriptions of longshore bars typically focus on their cross-shore asymmetry. A commonly used parameter for characterization is R_{tb}, which represents the ratio of the trough depth behind the bar (d_t) to the crest depth of the bar (d_b) (Wang et al., 2021), expressed as:

$$R_{tb} = d_t/d_b \tag{1}$$

The value of R_{tb} varies between longshore bars formed in different regions and at different slopes (Wang et al., 2021). It is an empirical value, generally considered to range between 1.4 and 1.7 (Evans, 1940; Keulegan, 1948; Drønen and Deigaard, 2007).

For longshore bars in the equilibrium state, there is a correspondence between the bar thickness and wave conditions. Starting from the ideal geometric morphology of longshore bars (Fig. 1C), the relationship between the thickness of the longshore bar (t_b), the crest depth (d_b), and the trough depth (d_t) behind the bar can be built, expressed as (Jiang et al., 2018):

$$t_b = d_t - d_b + \frac{(d_t - d_b)\tan\alpha}{\tan\theta} \tag{2}$$

where α is the seabed slope on which the bar forms, and θ is the landward bar slope.

Substitute Eq. (1) into Eq. (2), Eq. (2) can be simplified as Eq. (3):

$$t_b = (R_{tb} - 1)\left(\frac{\tan\alpha}{\tan\theta} + 1\right)d_b \tag{3}$$

Thus, the relationship between longshore bars and breaking waves can be expressed quantitatively.

2.3. Relationship between waves and winds

Waves are generated by winds blowing over the sea (or lake) surface, with stronger winds producing larger waves. Also, the size of waves is controlled by the duration and distance the wind blows on the water surface. Therefore, when studying wave size and wave characteristic parameters, fetch (F) is an important consideration. For a constant wind speed, larger fetch results in larger waves.

Waves cannot grow indefinitely as fetch increases, so waves that form under sufficiently long wind durations and across sufficiently large distances are called fully developed waves (Eyhavand-Koohzadi and Badiei, 2022). When the wind is stable and sustained, characteristics of the waves, such as period, height, and wavelength are considered constant throughout their propagation until the waves enter the deformation zone near the shore (Fig. 1A). These characteristic parameters can be directly calculated by wind speed. The specific calculation methods will be presented later.

Fully developed waves form in deep-water regions and their particles move as a circle, so they propagate toward the shore in a sinusoidal shape (Fig. 1A). In 1845, Airy provided a description of the shape of fully developed waves in deep-water regions under ideal conditions, so waves in this stage are also known as Airy waves. The wavelength of Airy waves (L_o) can be calculated from wind speed as follows (Airy, 1845):

$$L_o = \frac{2\pi U^2}{g} \tag{4}$$

where U is the wind speed at 10 m above sea level, and g is the gravitational acceleration (m/s^2).

The height of Airy waves is given by:

$$H_o = \frac{2U^2}{9g} \tag{5}$$

As waves propagate toward the shore, the water depth (d) gradually decreases. When the water depth becomes less than the depth of the wave base, the seabed begins to influence the waves, causing wave's deformation (Fig. 1A). Generally, the wave base is considered to be located at approximately half the wavelength below the water surface, which is $L_o/2$, although some researchers prefer slightly different values, such as $L_o/2.965$ (Le Roux, 2007a; Le Roux et al., 2010).

During the wave deformation process, the wavelength gradually decreases, while the wave height increases (Sakai and Battjes, 1980; Davidson-Arnott, 2011). The formula for calculating the wavelength after deformation is as follows (Le Roux, 2007a):

$$L_w = \sqrt{TL_b[g(0.5H_b + d)]^{\frac{1}{2}}} \tag{6}$$

where T is the period, L_b is the wavelength at the break, and H_b is the wave height at the break.

The formula for calculating the wave height after deformation is as follows (Le Roux, 2007b):

$$H_w = H_o[\mathrm{aexp}(\mathrm{b}H_o/L_o)] \tag{7}$$

where a and b are coefficients given by:

$$\mathrm{a} = 0.5875(d/L_o)^{-0.18}, d/L_o \le 0.0844 \tag{8}$$

$$a = 0.9672(d/L_o)^2 - 0.5013d/L_o + 0.9521, 0.0844 < d/L_o \leq 0.6 \quad (9)$$

$$a = 1, d/L_o > 0.6 \quad (10)$$

$$b = 0.0042(d/L_o)^{-2.3211} \quad (11)$$

It is important to note that for fully developed waves, their period (T) remains unchanged despite variations in wave shape. This characteristic distinguishes wave period from changes in wavelength and wave height. The period (T) of fully developed waves is related to wind speed (U), and the calculation formula is as follows:

$$T = \frac{2\pi U}{g} \quad (12)$$

The shallower the water, the more pronounced the wave deformation, which means the lower stability of the wave. During deformation, wave energy converges at the crest. Once it exceeds the critical threshold, the wave breaks, forming breaking waves. Based on data from CERC, a critical condition formula for wave breaking is provided (Le Roux et al., 2010):

$$H_b = d_b(-0.0036\alpha^2 + 0.0843\alpha + 0.835) \quad (13)$$

where d_b is the water depth at the break.

Thus, the relationship between the water depth (d_b) and the wave height (H_b) at the break can be expressed by Eq. (13). It is worth noting that Eq. (13) is an empirical formula validated for wave periods ranging from 1 s to 6 s and seabed slopes between 0° and 11.3°.

2.4. Calculation process of paleowind strength

After establishing the relationships among longshore bar, wave, and wind, the reconstruction of paleowind strength can be determined by using the thickness of a single-period longshore bar. The process requires geological data to obtain the bar thickness (t_b) and paleoslope (α). The steps are as follows: (1) Identify the maximum thickness of the longshore bar (t) from core or logging data, and applying a decompaction correction to determine its original thickness (t_0) during deposition. The method used to determined decompaction correction will be showed below. (2) Obtain the paleoslope (α) at the location of the longshore bar's position by using seismic or other geological data. (3) Substitute t_0 and α into Eq. (3) to calculate the water depth at the break (d_b). (4) Substitute d_b and α into Eq. (13) to determine the wave height of the break (H_b). (5) Set the initial value of wind speed U as 0, and then calculate Eq. (5) and Eqs. (7)–(11) simultaneously by gradually increase the value of U until the H_w and H_b values coincide. It is worthy to point out that, if the initial value U is set incorrectly, the solution might be wrong or incalculably.

The specific steps are illustrated in the flowchart in Fig. 2.

2.5. Verification of the method

The verification of a new technique or a new method is essential. The method should be tested against record data to determine whether the calculation result reflects reality accurately.

Therefore, a field study of Secret Harbour Beach in western Australia is selected as a modern example to verify the method proposed in this study. The field study was finished by Contardo and Symonds (2015), who revealed a morphological response on a barred beach to variable wave forcing over two summers and one spring. In this study, they measured the profile of sandbar in nearshore, which can be used to measure the thickness of the bars. Also, they recorded the wind speed data during their observation. Thus, we can use the thicknesses of sandbars to calculate the wind speed and compare to the record data to verify our method.

The Secret Harbour Beach is selected as a modern example for the following reasons: (i) it is located in a marine environment with no nearby river input, making it a wave-dominated system; (ii) tidal influence is negligible here since the spring and neap tidal ranges of 0.7 m and 0.2 m respectively; (iii) the area consists of sandy beaches, with a median grain size of 0.22 mm, which satisfies the assumptions of the self-organizational model.

The study conducted by Contardo and Symonds (2015) includes three periods data: summer 2012, spring 2012, and summer 2013. We used the published data from their work to obtain the average thickness of longshore bar profiles for each of these periods, and calculated the corresponding average wind speeds. Based on the field conditions described in their paper, the parameter α was assigned a value of 1.72° according to local measurements when calculating wind speed from sandbar thickness. The parameters θ and R_{tb} are empirical values and are

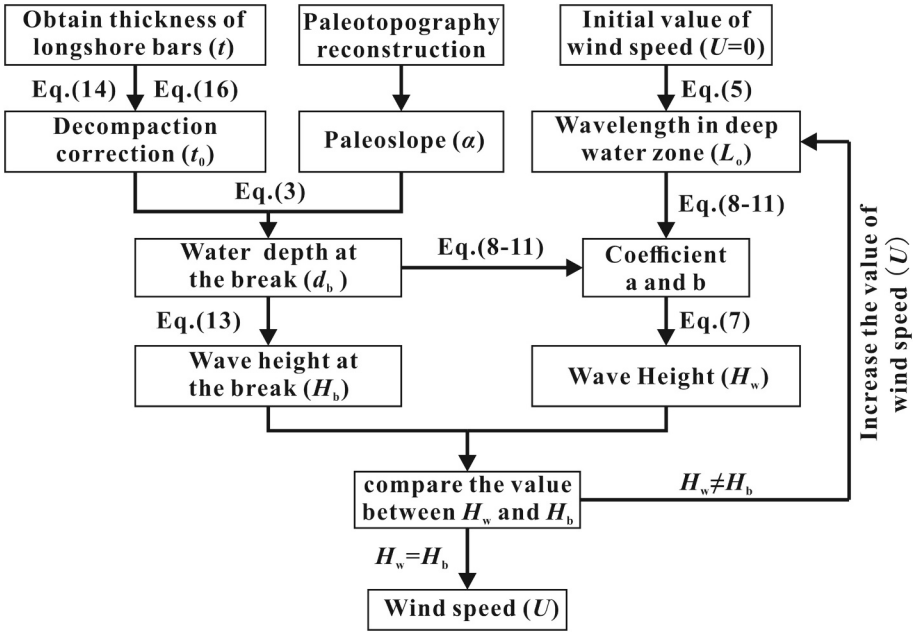

Fig. 2. Flowchart of peleowind strength restoration.

therefore θ set to 32° and R_{tb} to 1.6, which consistent with the values used later in this study. The calculation results are shown in Table 1.

When comparing the calculated wind speeds to the average values of the measured wind speeds, the maximum difference between them is 0.531 m/s of the data in summer 2013. This difference is significantly smaller than the natural variability of wind speeds observed in the field, which are all over 15 m/s. Therefore, it can be concluded that the calculated wind speeds are generally consistent with the real wind speeds, indicating that the paleowind reconstruction method proposed in this study is feasible.

3. Application to the Pingbei slope zone, Xihu Sag

3.1. Background of study area

The Pingbei Slope Zone of the Xihu Sag is located in the northeastern part of the East China Sea Shelf Basin and represents a key oil and gas rich region within the basin. The Pinghu Formation, dates ~42.5–32.0 Ma, is a significant oil and gas reservoir within the Xihu Sag (Abbas et al., 2018; Su et al., 2019; Wu et al., 2022; Guo et al., 2024; He et al., 2024; Li et al., 2024b). Based on well-log and seismic data, the Pinghu Formation has been divided into five third-order sequences.

Through core facies and log analysis, the fourth third-order sequence of the Pinghu formation (SQ4, 37.2–35.5 Ma) is the focus of this study. This period can be further divided into two systems tracts: the Transgressive Systems Tract (TST) and the Highstand Systems Tract (HST). In the TST, single sand body thicknesses are relatively thin and coal seams are less frequent, so the depositional environment leans more toward a shoreline setting. During this period, longshore bar deposits, which are favorable for paleowind reconstruction, are relatively abundant. In contrast, the HST is characterized by thicker sand bodies and an increase in the quantity of coal seams, which implies a depositional environment dominated by barrier island-lagoon system. During the HST, longshore bar deposits are less frequent and less suitable for paleowind reconstruction (Fig. 3).

Based on the Cenozoic Pacific sea-level reconstruction of Miller et al. (2020), the East China Sea Shelf Basin experienced two significant marine transgressions during the Pinghu Formation period. The first was a rapid sea-level rise at approximately 40.7 Ma, and the second was a gradual rise at around 36.7 Ma, which aligns with the SQ4 identified in this study. During this period, a sea-level rose by about 20 m, providing water depth conditions conducive to the development of longshore bars.

Since initiation of exploration and development in the Xihu Sag, extensive research on the sedimentary systems of the Pinghu Formation has been conducted. Although opinions vary, the widely accepted consensus is that the Pinghu Formation consists of coal-bearing strata representing a transitional marine-terrestrial depositional environment, with a significant tidal influence (Abbas et al., 2018; Cai et al., 2019; Li et al., 2022; Wang et al., 2024; Xu et al., 2024).

This study reinterprets the sedimentary characteristics of the Pinghu Formation based on approximately 150 m of core data from 17 wells. Based on rock color, grain size, structure, and texture of the core, four primary sedimentary facies have been identified within the study area: bar, barrier island, tidal channel, and lagoon (Fig. 4).

Table 1
Comparison between calculated wind speeds and recorded wind speed of Secret Harbour Beach in Australia (according to Contardo and Symonds, 2015).

Date	Average thickness of longshore bar (m)	Average value of measured wind speed (m/s)	Calculated wind speed (m/s)	Difference
Summer 2012	~0.874	~6.419	6.802	0.383
Spring 2012	~0.861	~6.533	6.751	0.218
Summer 2013	~1.065	~6.977	7.508	0.531

3.2. Paleowind strength estimation

3.2.1. Identification of fossil longshore bars

Identifying longshore bars is the first and foundational step in reconstructing paleowind strength. As a type of shoreline bars, longshore bars represent the outermost bars, situated farthest from the shore. Shoreline bars form in nearshore environments far from sediment sources, and are shaped by waves, which result in strong hydrodynamic conditions. Thus, longshore bars exhibit high compositional maturity ($Q/(R + F) > 70$ %, where Q is quartz, R is lithic and F is feldspar). Also, grain size of longshore bars typically ranges from fine-grained to medium-grained sandstone, with occasional lenses of fine conglomerate.

A complete longshore bar deposit corresponds to a parasequence, and its top and bottom boundaries marked by mud, which indicates the flooding surfaces (Wang, 2016). This cycle reflects a gradual shallowing water depth, so the longshore bar sand bodies typically exhibit a coarsening-upward trend in the vertical profile. Occasionally, a fining–coarsening–fining composite grain-size pattern may appear, indicating a depositional environment where wave energy gradually weakened after bar formation.

Based on previous research by Taylor and Ritts (2004) and core data in study area, we establish a typical succession of lithofacies of an idealized longshore bars parasequence. An idealized vertical sequence of longshore bars commonly includes, from bottom to top: massive mudstone, usually offshore mudstone, represents suspension load fallout mud, indicate deep water; lenticular to wavy ripple laminated siltstone, pelitic strip silty to fine sandstone, ripple-laminated fine sandstone, planar cross-bedded fine to medium sandstone, massive medium sandstone, parallel-bedded medium to coarse sandstone, low angle cross-bedded medium sandstone, parallel-laminated fine conglomerate, trough cross-bedded medium sandstone, and wavy ripple to lenticular laminated siltstone, culminating in massive mudstone (Fig. 5).

It should be noted that due to the migratory nature of sandbars, superposition of multiple longshore bars often occurs. When such superposition is present, the paleowind reconstruction method proposed in this study must be applied using the thickness of an individual longshore bar rather than the cumulative thickness of multi-phase stacked bars. Identification of single-phase sandbars should follow the facies sequence criteria described earlier in the manuscript. For example, if the sedimentary structure displays a marked shift in hydrodynamic energy—such as a transition from parallel laminate to lenticular laminate—this should be interpreted as representing two distinct sandbar-forming events.

In addition, since longshore bars form in relatively deeper water, a decline in wind strength and wave energy may lead to earlier-formed longshore bars being buried by fine-grained sediments, resulting in the formation of a thin mudstone layer. Even if longshore bars from different periods become superimposed, the presence of a black mudstone layer between them can serve as a distinguishing marker. The mudstone should be used as the basis for separating individual depositional events during the identification of single-phase longshore bars.

Due to the limited amount of core data, reconstructing paleowind usually requires identifying multiple phases of longshore bars in well-log data. Therefore, existing methods for identifying shoreline bars in cores and well-log data can also be applied to longshore bars (Jiang et al., 2011). Longshore bars exhibit a coarsening upward trend overlain by a fining upward trend, which could be discernible in well-log data with a vertical resolution of 0.125 m. On gamma-ray (GR) logs, longshore bars typically appear as box-shaped or funnel-shaped curves (Fig. 5). Based on previous research on modern sediments and a statistical analysis within the study area, the thickness of longshore bars generally ranges from 0.5 to 3.5 m, rarely exceeding 5 m.

During the identification process, longshore bar phases should be

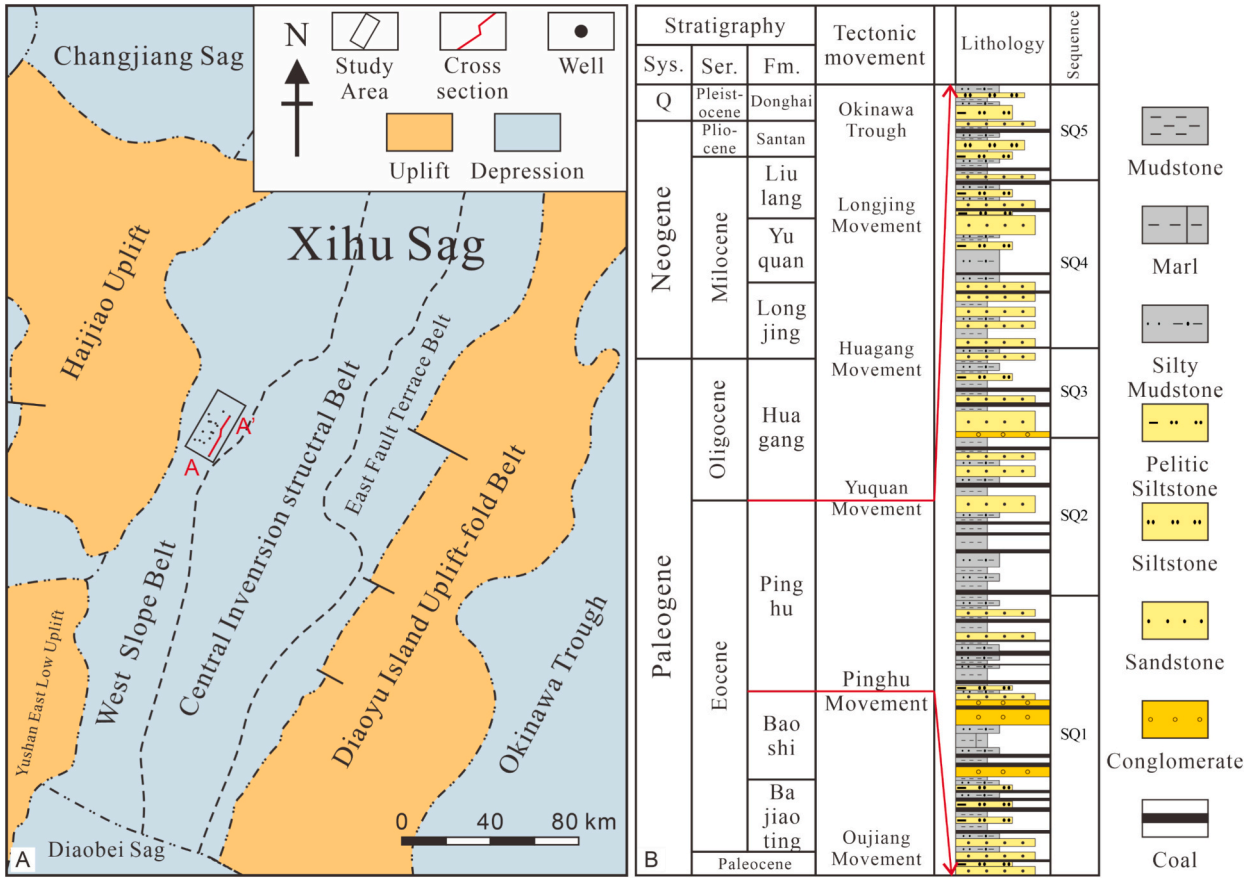

Fig. 3. (A) Tectonic map of Xihu Sag, East China Shelf Basin (modified from Liu, 2020). (B) Generalized stratigraphic column of Xihu Sag, East China Sea Shelf Basin showing tectonic evolution, lithologies and sequence (modified from Chang et al., 2021; Yan et al., 2024). Abbreviation: Sys.: System; Ser.: Series; Fm.: Formation; Q: Quaternary.

labeled in accordance with the principle of chronostratigraphic correlation. Each bar should then be analyzed sequentially to calculate its corresponding paleowind strength, thereby reconstructing the temporal variations in ancient wind strength. Based on the paleotopography reconstructions, four wells (cross-section AA′) were selected (Fig. 6). A total of 35 longshore bars were identified within these wells.

3.2.2. Decompaction correction of bar thicknesses

The study area lies at a depth exceeding 4000 m, where compaction effects are significant, resulting in the thickness of longshore bars identified in well logs being less than their original thickness (Jiang et al., 2009). Therefore, to accurately reconstruct paleowind strength using the thickness of longshore bars, a decompaction correction must be applied to derive the initial bar thickness.

During the compaction process, the volume reduction in rock is primarily due to compression of intergranular pore spaces, leading to a significant decrease in porosity with increasing depth. Assuming the framework grains of the rock remain undeformed during compaction, and only the pore space is reduced, the pre-compaction thickness of the bar can be approximated by the following equation (Jiang et al., 2018):

$$t_0 = \frac{1-\varphi}{1-\varphi_0} t \tag{14}$$

where t_0 is the ancient thickness of the bar, φ_0 is the ancient porosity of the bar, φ is the current porosity of the bar, and t is the current thickness of the bar.

Because of the limited amount of data, porosity data of both the measured porosity (φ) and the initial porosity (φ_0) for each identified longshore bar may not be available. However, since porosity typically decreases with depth following a predictable trend, the initial porosity (φ_0) can be calculated using a compaction equation, which is as follows (Jiang et al., 2009):

$$\varphi = \varphi_0 \exp(-Ch) \tag{15}$$

where C is compaction coefficient, and h is the burial depth of the bar.

The values of C and φ_0 can be determined using measured porosity data by plotting a curve of porosity versus depth and fitting the relationship. Using measured porosity data from Well B1, a compaction equation for the Pingbei slope zone in the Xihu Sag was derived through curve fitting (Fig. 7):

$$\varphi = 52.2393 \exp(-0.0003h) \tag{16}$$

Therefore, t_0 of longshore bars at different depths can be calculated by Eq. (14) and Eq. (16).

3.2.3. Value of paleoslope

The paleoslope (α) is an essential parameter needed for reconstructing paleowind strength, as its magnitude influences both the wave deformation process and the formation of longshore bars. A steeper slope results in more intense wave deformation and a greater energy release during wave breaking (Wang and Zou, 2016). The average continental shelf slope is approximately 0.1°, while longshore bars typically develop in the nearshore region of the inner continental shelf (Jiang et al., 2020; Zhu, 2020). Modern observations and flume experiments show that the inner continental shelf often displays a gradual steepening of its slope onshore, suggesting that the seabed slope near the shore is relatively steep (Bruun, 1962; Wang and Muto, 2021).

In order to study the range of α, a survey of slopes associated with

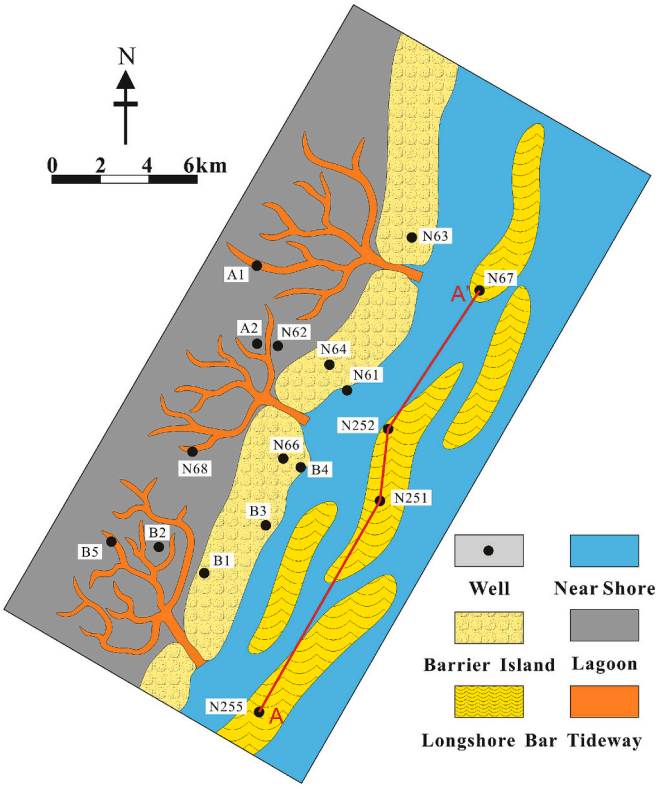

Fig. 4. Sedimentary facies map of SQ4 sequence of the Pinghu Formation of Pingbei slope zone.

longshore bar development in modern deposits is included in this study. For example, in Chesapeake Bay in the United States, the slope at the location of longshore bars is approximately 0.0052 or less, while the nearshore slope of Terschelling Island off the northwest coast of the Netherlands is 0.0056 (Dolan and Dean, 1985; Ruessink and Kroon, 1994). In Secret Harbour Beach in west Australia, the slope of the sandy beach is about 0.03 (~1.72°) (Contardo and Symonds, 2015). Davidson-Arnott (2013) thinks sandbar generation should occur with a nearshore bed slope in the range of 0.005–0.03 (~0.3°–1.72°). We assume an average slope of about 1° (~0.017). Notably, when the error in α values is relatively small (<1° approximately), its influence on the paleowind speed (U) calculations is negligible, as will be demonstrated later in this text.

3.2.4. Calculation of paleowind strength

After performing decompaction corrections for the t_0 of longshore bars and using the average α in the study area, paleowind strength can be calculated. First, use the t_0 to determine the corresponding d_b by using Eq. (3), assuming $R_{tb} = 1.6$ and $\theta = 32°$. Once the d_b is obtained, the wave's characteristics can be derived further: use Eq. (13) to calculate the wave height of breaker (H_b). Finally, an iterative computational method using Eqs. (7)–(11) determines the value of U when H_b equals H_w.

Using multiple longshore bar data from well logs, the paleowind strength variation in the study area from 37.2 to 35.5 Ma is reconstructed (Fig. 8). The results indicate that wind speeds during this period ranged from 8.76 to 19.71 m/s. When exam paleowind strength through the time, paleowind variations in the transgressive systems tract (TST) were relatively intense, showing significant high-frequency shifts with four distinct peaks and troughs (Fig. 8). The maximum wind speed variation reached 10.95 m/s. In contrast, variations in paleowind strength during the highstand systems tract (HST) were relatively moderate, with less pronounced and irregular fluctuations.

4. Discussion

4.1. Effectiveness of the method

When waves propagate shoreward, they generally undergo multiple breaks. Based on the characteristics of nearshore bars, the wave transformation zones can be divided into the storm zone, shoaling zone, breaker zone, reformation zone, surf zone, and swash-backwash zone (Jiang et al., 2015). Among these, the breaker zone and the surf zone exhibit greater energy variation and more sediment discharge, which often leads to the formation of thicker "bars". In contrast, the shoaling and reformation zones are associated with less sediment discharge, typically resulting in thinner "beaches" (Wang, 2016). The swash-backwash zone can also create nearshore bars that serve as valuable geological data for reconstructing paleowind strength (Wang et al., 2018a).

The methodology for reconstructing paleowind strength proposed in this study requires researchers to focus on longshore bars, which are located at the outermost, farthest offshore position. This is because the longshore bars are formed during the first break in waves, where the relationship between H_b and d_b can be quantitatively expressed by Eq. (13). Those bars formed closer to the shore result from subsequent wave-breaking events, so they do not align with the assumptions of wave energy and morphology outlined earlier in this study.

In real wave systems, sandbars often migrate in response to sea-level fluctuations, which can lead to the superposition of multiple sandbar bodies. It is important to note that the longshore bars used for paleowind reconstruction must be single-phase bars; the cumulative thickness of superimposed longshore bars is not applicable to the method proposed in this study. This is because the quantitative relationship assumed between longshore bar thickness and break is derived based on the formation process of an individual sandbar event. Therefore, the method is not valid for multi-phase stacked longshore bars. For such cases, the identification of single-phase longshore bars should be conducted according to the criteria described in Section 3.2.1 of this paper.

Since irregular coastlines and seabed undulations interfere with wave propagation direction, waves may not always travel perpendicular to the shoreline. When waves approach at oblique or parallel angles, refraction occurs, altering the energy distribution of the waves. In such cases, the relationship between bars and wave energy diverges from the ideal deposition model of longshore bars discussed earlier. Therefore, the method for reconstructing paleowind strength based on longshore bar thickness assumes waves approach the shoreline perpendicularly or at a high angle.

According to the self-organizational model of longshore bars, their formation results from the reciprocal transportation of sediments by waves. The correlation between bar thickness and paleowind strength emerges after prolonged action by a wind field with stable intensity (Moore et al., 2003; Coco and Murray, 2007). Consequently, the paleowind reconstruction method presented in this study is applicable only to longshore bars formed under normal weather conditions, which usually last for a longer time. On the other hand, it does not apply to those resulting from infrequent events such as typhoons or storms.

4.2. Inherent uncertainty considerations

The quantitative paleowind strength reconstruction method proposed in this study involves steps and relationships valid under idealized conditions. Some derivations rely on assumptions and approximations, which inherently introduce potential errors. To better utilize this method, researchers should thoroughly understand each step of the process and the influence of each parameter on the final results. This understanding can be achieved through single-parameter sensitivity analysis, wherein one parameter is varied at a time while others are held constant. By examining how variations in a single parameter affect the outcome, researchers can quantitatively assess the sensitivity of the

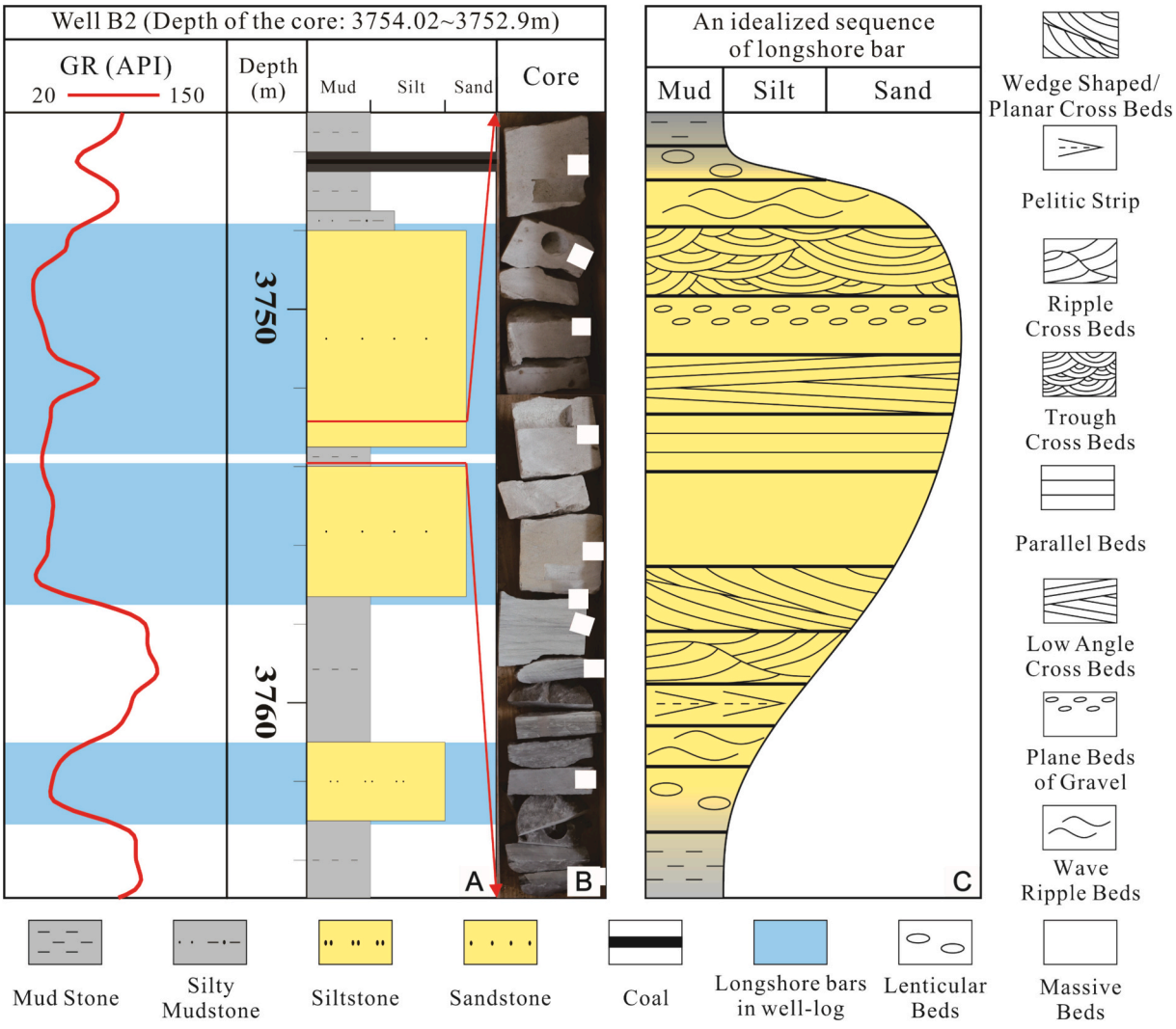

Fig. 5. Lithofacies succession within an idealized longshore bar deposit. (A) Well-log of well B2, in which identified 3 longshore bars. (B) Rock core of well B2 at 3754.02–3752.9 m, which presents as a single phase of longshore bar. (C) An idealized vertical sequence of longshore bars.

results to that parameter and evaluate the method's tolerance to errors in its measurement.

A sensitivity analysis was conducted on the parameters used in the paleowind strength reconstruction method. The parameters t_b and α are measured based on field data from the study area, while R_{tb} and θ are derived empirically. Among these parameters, t_b directly correlates with the calculated U. Hence, accurate measurement of t_b is crucial because its errors significantly affect the U results (Fig. 9A).

Assuming accurate t_b values, the influence of slope α on U is minimal. For instance, as shown in Fig. 9B, when α varies within the range of 0.05–1.5°, the wind speed error remains below 0.5 m/s.

The parameter R_{tb}, based on experimental and modern sedimentary observations, also influences the results. Fig. 9C illustrates that a smaller R_{tb} value leads to more pronounced variations in the outcome of U. However, when R_{tb} exceeds 2, the sensitivity of U to R_{tb} decreases significantly, and within the range of R_{tb} = 2.5–3.0, U variations are limited to about 1 m/s.

Lastly, θ, represents the landward slope of bars (a natural slope formed during sediment accumulation), theoretically approaching the angle of repose (Thornton et al., 1996). According to Fig. 9D, variations in θ between 10° and 40° result in U variations of approximately 0.3 m/s, indicating that uncertainties in θ are a less significant source of calculational error in U.

4.3. Comparison with existing methods

In previous proposed methods for reconstructing paleowind strength, obtaining paleofetch is an essential and indispensable step. However, in marine basins, accurately measuring paleofetch proves challenging due to the method itself. For lacustrine basins, reconstructing paleowind strength begins by determining the ancient shoreline location using geological data. Then, the distance is measured along the wind direction from the position of the paleo-longshore bars to the edge of the water body, approximating the paleofetch.

This approach, however, is hard to implement in marine basins. Due to the vast area of the ocean, the distance between the measurement point and the basin boundary often greatly exceeds the wind's actual fetch, rendering such measurements unreflective of historical wind conditions. With all other factors constant, larger fetch leads to smaller reconstructed paleowind strength, following an inverse proportional relationship (Wang et al., 2021). This suggests that for a given longshore bar thickness, there is a theoretical minimum wind speed corresponding to an infinitely large fetch. In other words, while a small bar can result from strong wind with a short fetch, a large bar cannot form in gentle wind condition. Consequently, the paleowind strength corresponding to a longshore bar of the same thickness in a lake basin is likely to be greater than that in an ocean basin.

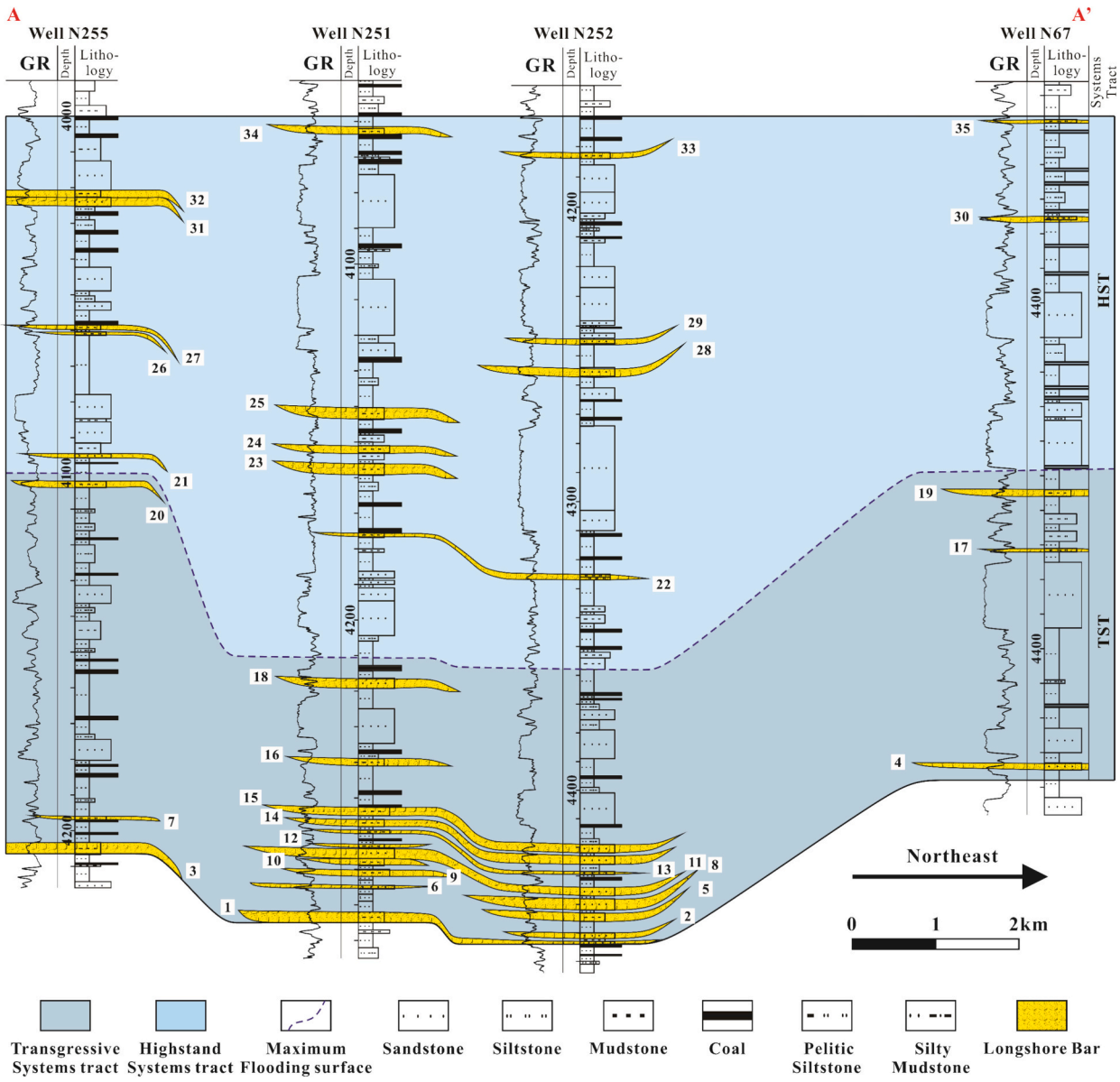

Fig. 6. SQ4 of Pinghu formation (37.2–35.3 Ma) cross-section in Pingbei Slope Zone in Xihu Sag (Section AA′ in Fig. 4).

4.4. Application to the Pinghu Formation in Xihu Sag

The paleowind strength reconstruction for the Pinghu Formation in the Xihu Sag provides a supplement to the paleoclimate understanding of the region, filling a gap in the knowledge of its ancient atmospheric circulation. The calculated paleowind speed range for the West Slope Belt of the Xihu Sag is between 8.76 and 19.71 m/s. Since there has been no prior paleowind strength reconstruction conducted specifically for the Xihu Sag, this study refers to the results of Jiang et al. (2018), who reconstructed paleowind strength in the Dongying Depression using longshore bar thickness. Jiang's reconstruction yielded wind speeds ranging from 6.9 to 18.2 m/s. Considering that the Dongying Sag represents a paleo-lacustrine setting while the Xihu Sag represents a paleo-marine setting, it is reasonable that both the minimum and maximum wind speeds reconstructed for the Xihu Sag are slightly higher than those from the Dongying Sag. This comparison provides additional support for the validity of the paleowind strength reconstruction method proposed in this study.

In applying the paleowind strength reconstruction method proposed in this study, a total of 35 data points from four wells were selected—20 from the transgressive systems tract and 15 from the highstand systems tract (Fig. 6). Besides, the duration of the transgressive phase is shorter than that of the highstand phase, which makes the variation in wind strength during the transgression appears to be more pronounced. This phenomenon arises from the greater water depth during the transgressive period, which enhanced the preservation potential of longshore bars. In other words, more wave-generated longshore bars were preserved during the transgressive phase, resulting in more frequent paleowind strength fluctuations captured in the dataset. In contrast, fewer bars were preserved during the highstand phase, leading to a relatively smoother wind strength variation curve. Thus, the paleowind strength results obtained using this method should not be used as direct evidence to infer correlations between sea-level fluctuations and atmospheric circulation patterns.

4.5. Implication

Quantitatively reconstructing information from geological records has long been one of the most challenging tasks in the field of geology. It is important to emphasize that the paleowind strength reconstructed

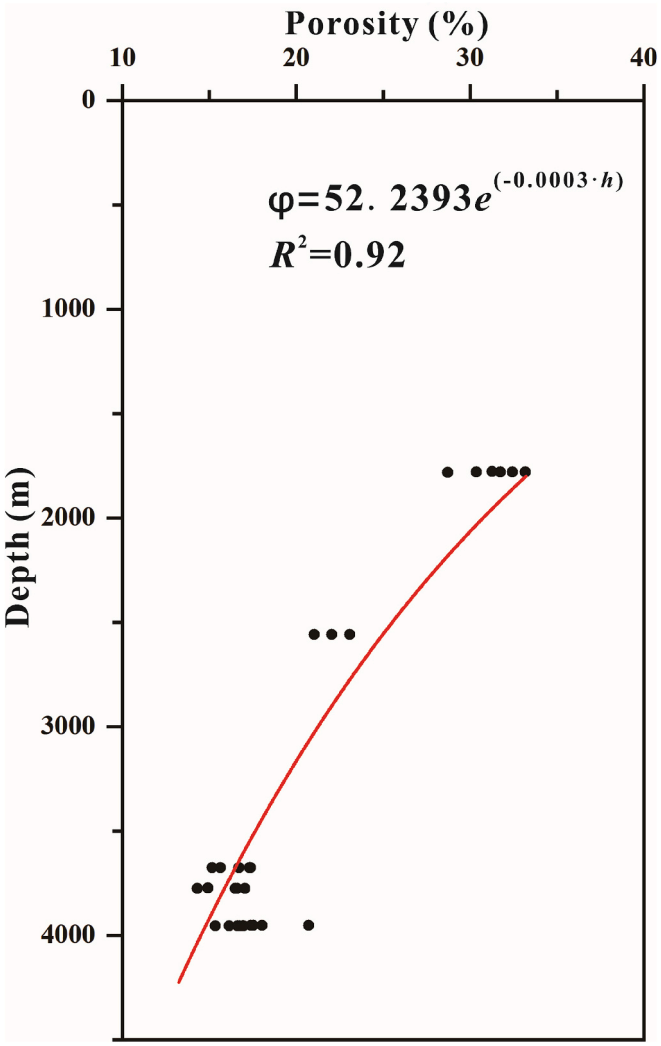

Fig. 7. Fitting diagram of compaction curve.

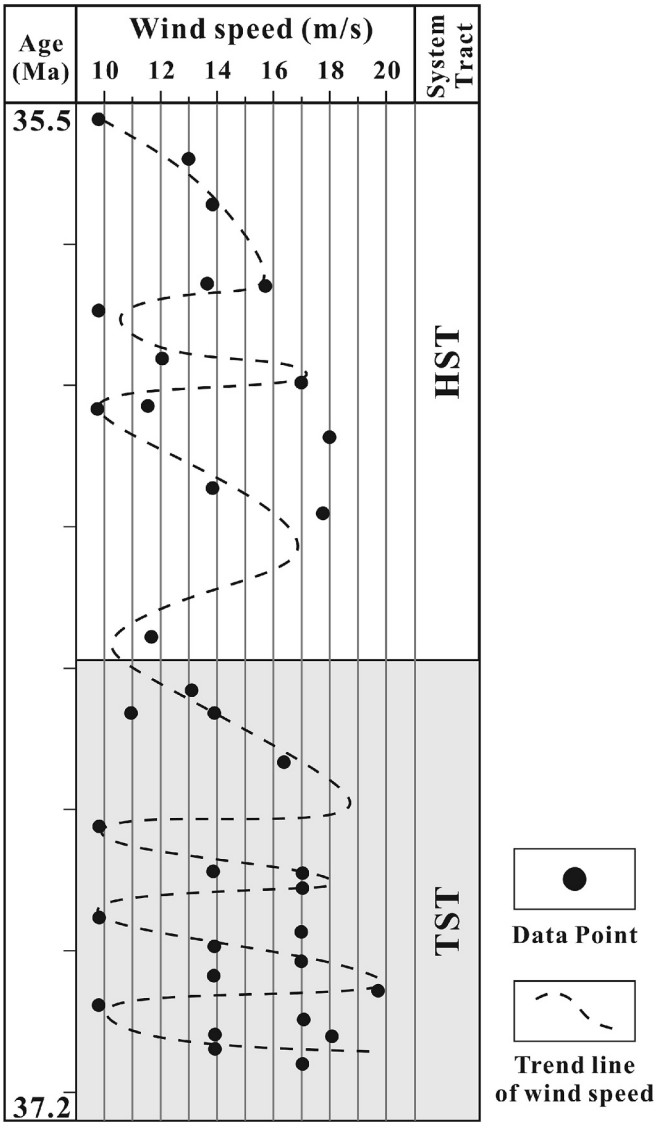

Fig. 8. Paleowind strength variation curve of Pinghu Formation in Pingbei slope zone of Xihu Depression at SQ4.

using the method presented in this study should be interpreted as the maximum wind strength in the region at the time, rather than the average wind strength. This is because the geological features used in the reconstruction are longshore bars, located at the outermost position among a series of parallel bars. On one hand, the outer longshore bar corresponds to the point where waves first break—this is when wave energy is at its peak. On the other hand, because the outermost longshore bar is situated farthest from the shoreline, the wind strength at that location is theoretically higher than that in more nearshore environments.

Due to the limitations of geological data, simplifications and assumptions are inevitable. However, we believe that the trend of the paleowind strength reconstructed by this method should generally be consistent with the actual paleoclimatic conditions. One of the primary purposes of proposing this quantitative reconstruction method is to stimulate reflection and discussion, encouraging more researchers to engage in the validation and refinement of paleowind reconstruction techniques. This will eventually lead to the development of more effective and accurate methods for determining paleowind strength.

5. Conclusion

In paleoclimate research, studies focusing on ancient wind fields are relatively scarce. Previous work, based on the self-organizational model theory of bars, used waves as a connection to establish an equivalence between longshore bars and wind field intensity. This method enabled bar deposits in geological records to serve as materials for studying ancient wind fields. However, due to the limitation in measureing paleofetch, traditional methods are primarily applicable to ancient lakes and difficult to determine in marine settings. This study incorporates the theory of fully developed waves, redefining the relationship between waves and wind fields, making it feasible to reconstruct the strength of paleowinds in marine environments using the thickness of longshore bars.

The proposed method is based on assumptions and approximates approximations, applicable in scenarios where wind direction is perpendicular or intersects the shoreline at a high angle. Also, the wind field should be stable over a sufficiently long duration, so both wave size and longshore bar thickness would reach equilibrium. Although the method relies on an idealized model, its strength lies in requiring relatively few parameters and its simplicity compared to existing methods. Meanwhile, the assumptions and approximations inevitably introduce some errors. Sensitivity analysis shows that this method is highly sensitive to the thickness of longshore bars (t_b) and the ratio of trough depth to bar crest depth (R_{tb}), making accurate determination of these parameters critical.

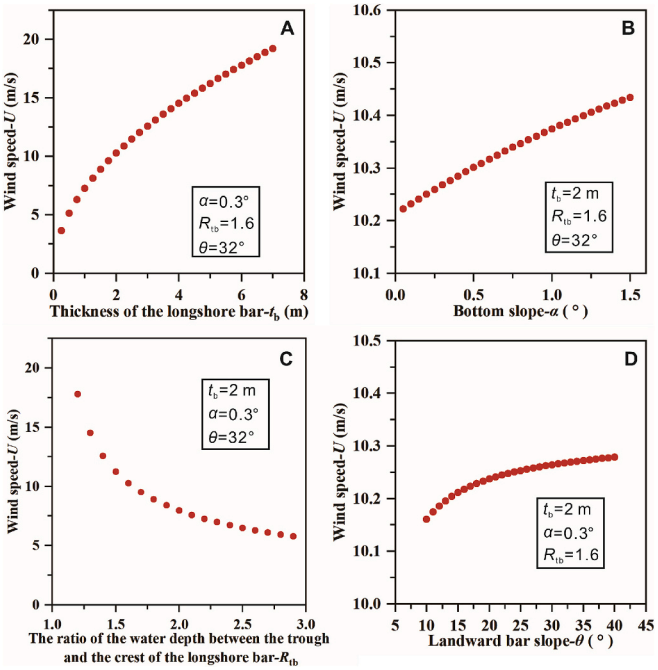

Fig. 9. The effects of four parameters (t_b, α, R_{tb}, θ) on the calculated wind speed (U). (A) When t_b ranges from 0.25 to 7 m, U ranges from 3.63 to 19.21 m/s. (B) When α ranges from 0.05 to 1.5°, U ranges from 10.22 to 10.43 m/s. (C) When R_{tb} ranges from 1.1 to 2.9 m, U ranges from 25.15 to 5.77 m/s. (D) When θ ranges from 10 to 40°, U ranges from 10.16 to 10.28 m/s.

Wind fields, as a manifestation of atmospheric circulation in localized areas, are essential components of climate research. Reconstructing ancient wind fields from sedimentary records is a valuable supplement to traditional methods of paleogeography and paleoclimate research. By considering wind as a geological driving force and starting from its control over sedimentary processes, this study provides a quantitative approach to reconstructing wind field magnitude and its variations millions of years ago. This approach not only facilitates detailed reconstruction of paleogeographic environments in specific basins but also offers insights into the history of global atmospheric conditions.

List of symbols

a	Coefficient used in calculation of H_w, 1
b	Coefficient used in calculation of H_w, 1
C	Coefficient of consolidation, m^{-1}
d	Water depth, m
d_b	Water depth at the bar crest/Water depth at the breaker zone, m
d_t	Water depth at the landward trough, m
F	Fetch, m
g	Gravitational acceleration, m/s^2
H_b	Wave height at the breaker zone, m
H_o	Wave height in the deep water, m
H_w	Wave height in any water depth, m
h	The burial depth of the longshore bar, m
L_b	Wave length at the breaker zone, m
L_o	Wave length in the deep water, m
L_w	Wave length in any water depth, m
R_{tb}	The ratio of the water depth between the trough and the crest of the longshore bar, 1
T	Fully developed wave period, s
t	Current thickness of the longshore bar, m
t_0	Ancient thickness of the longshore bar, m
t_b	Thickness of the longshore bar, m
U	Wind speed at 10 m above base level, m/s
α	Bottom slope, °
θ	Landward bar slope, °
φ	Current porosity of the longshore bar, %
φ_0	Ancient porosity of the longshore bar, %

CRediT authorship contribution statement

Jinlin Chen: Writing – review & editing, Writing – original draft, Software, Methodology, Investigation, Formal analysis, Data curation, Conceptualization. **Junhui Wang:** Writing – review & editing, Validation, Supervision, Resources. **Guofeng Yin:** Resources. **Yang Wu:** Formal analysis, Data curation. **Zhengming Dai:** Data curation. **Yonglin Li:** Investigation, Data curation. **Jinhao Ma:** Writing – review & editing, Data curation. **Zaixing Jiang:** Writing – review & editing, Resources, Project administration. **Jie Xu:** Writing – review & editing, Supervision.

Declaration of competing interest

The authors declare that they have no known competing financial interests or personal relationships that could have appeared to influence the work reported in this paper.

Acknowledgments

We thank the CNOOC Shanghai Branch and the SINOPEC Shanghai Offshore Oil & Gas company for providing research funding, access to the data and permission to publish. This work was supported by the National Natural Science Foundation of China (42172108, 41702104) and the research project of Chinese Academy of Sciences (THEMSIE04010101). We thank Jianing Jiang for helpful discussion on reversion of paper. We thank the Editor Dr. Giorgio Basilici, the Journal Manager Parthiban Rajendran and three anonymous reviewers for their fruitful comments during the revision process, which resulted in an improved version of the manuscript. We have no conflict of interest to declare.

Data availability

The data that has been used is confidential.

References

Abbas, A., Zhu, H., Zeng, Z., Zhou, X., 2018. Sedimentary facies analysis using sequence stratigraphy and seismic sedimentology in the Paleogene Pinghu Formation, Xihu Depression, East China Sea Shelf Basin. Marine and Petroleum Geology 93, 287–297. https://doi.org/10.1016/j.marpetgeo.2018.03.017.

Adams, K.D., 2003. Estimating palaeowind strength from beach deposits. Sedimentology 50, 565–577. https://doi.org/10.1046/j.1365-3091.2003.00565.x.

Airy, G.B., 1845. Tides and Waves. In: Encyclop Metrop Article, 192, pp. 241–396.

Bauer, B.O., Davidson-Arnott, R.G.D., Hesp, P.A., Namikas, S.L., Ollerhead, J., Walker, I. J., 2009. Aeolian sediment transport on a beach: Surface moisture, wind fetch, and mean transport. Geomorphology 105, 106–116. https://doi.org/10.1016/j.geomorph.2008.02.016.

Biausque, M., Grottoli, E., Jackson, D.W.T., Cooper, J.A.G., 2020. Multiple intertidal bars on beaches: a review. Earth-Science Reviews 210, 103358. https://doi.org/10.1016/j.earscirev.2020.103358.

Bruun, P., 1962. Sea-level rise as a cause of shore erosion. Journal of the Waterways and Harbors Division 88, 117–130.

Cai, H., Qin, L., Liu, Y., 2019. Differentiation and coupling model of source-to-sink systems with transitional facies in Pingbei slope of Xihu sag. Earth Science 44, 880–897 (in Chinese with English abstract).

Chai, B., Liu, C., Hu, Y., Zhang, P., Xing, B., Hu, C., 2024. Critical condition for wind-driven wave breaking with the effect of surface tension. Ocean Engineering 311, 118913. https://doi.org/10.1016/j.oceaneng.2024.118913.

Chang, Y., Duan, D., Zhang, L., Ding, F., Bao, Q., 2021. Quantitative characterization of the depositional system in Gas field A, Pinghu slope belt, Xihu Sag and its bearing on periodicity of sea level changes. Marine Geology & Quaternary Geology 41, 12–21 (in Chinese with English abstract). 10.16562/j.cnki.0256-1492.2020081302.

Chen, Y., Liu, X., Li, J., Liu, X., Ou, X., 2024. Impact of millennial-scale fluctuations of the Siberian High on Holocene aeolian activity: Insights from Lake Ailike in arid Central

Asia. Global and Planetary Change 242, 104593. https://doi.org/10.1016/j.gloplacha.2024.104593.
Coco, G., Murray, A.B., 2007. Patterns in the sand: from forcing templates to self-organization. Geomorphology 91, 271–290. https://doi.org/10.1016/j.geomorph.2007.04.023.
Contardo, S., Symonds, G., 2015. Sandbar straightening under wind-sea and swell forcing. Marine Geology 368, 25–41. https://doi.org/10.1016/j.margeo.2015.06.010.
Davidson-Arnott, R., 2011. Wave-dominated coasts. In: Treatise on Estuarine and Coastal Science. Elsevier, pp. 73–116. https://doi.org/10.1016/B978-0-12-374711-2.00305-3.
Davidson-Arnott, R., 2013. Nearshore bars. In: Shroder, J., Sherman, D.J. (Eds.), Treatise on Geomorphology, 18, pp. 419–448.
Davidson-Arnott, R.G.D., Bauer, B.O., 2009. Aeolian sediment transport on a beach: Thresholds, intermittency, and high frequency variability. Geomorphology 105, 117–126. https://doi.org/10.1016/j.geomorph.2008.02.018.
Dolan, T.J., Dean, R.G., 1985. Multiple longshore sand bars in the upper Chesapeake Bay. Estuarine, Coastal and Shelf Science 21, 727–743. https://doi.org/10.1016/0272-7714(85)90069-1.
Drønen, N., Deigaard, R., 2007. Quasi-three-dimensional modelling of the morphology of longshore bars. Coastal Engineering 54, 197–215. https://doi.org/10.1016/j.coastaleng.2006.08.011.
Dyhr-Nielsen, M., Sørensen, T., 1970. Some sand transport phenomena on coasts with bars. In: Coastal Engineering 1970. https://doi.org/10.1061/9780872620285.054. Presented at the 12th International Conference on Coastal Engineering, American Society of Civil Engineers, Washington, D.C., United States, 855–865 pp.
Eastwood, E.N., Kocurek, G., Mohrig, D., Swanson, T., 2012. Methodology for reconstructing wind direction, wind speed and duration of wind events from aeolian cross-strata. Journal of Geophysical Research: Earth Surface 117, 2012JF002368. https://doi.org/10.1029/2012JF002368.
Evans, O.F., 1940. The low and ball of the east shore of Lake Michigan. Journal of Geology 48, 476–511.
Eyhavand-Koohzadi, A., Badiei, P., 2022. Experimental study on the growth and conversion of duration- and fetch-limited wind waves in water of finite depth. Ocean Engineering 266, 113020. https://doi.org/10.1016/j.oceaneng.2022.113020.
Favaro, E.A., Balme, M.R., McNeil, J.D., Fawdon, P., Davis, J.M., Grindrod, P.M., Lewis, S.R., 2024. Periodic Bedrock Ridges at Oxia Planum and Chryse Planitia, Mars: evidence for widespread aeolian erosion of an ancient surface by regional paleowinds. Earth and Planetary Science Letters 626, 118522. https://doi.org/10.1016/j.epsl.2023.118522.
Ge, J., Guo, Z., Zhao, D., Zhang, Y., Wang, T., Yi, L., Deng, C., 2014. Spatial variations in paleowind direction during the last glacial period in north China reconstructed from variations in the anisotropy of magnetic susceptibility of loess deposits. Tectonophysics 629, 353–361. https://doi.org/10.1016/j.tecto.2014.07.002.
Goda, Y., 1970. A synthesis of breaker indices. Proceedings of the JSCE 1970, 39–49 (in Japanese).
Guo, G., Li, X., Han, Y., Li, F., Chen, Y., Li, L., 2024. Diagenetic facies types and their control on reservoirs of eocene pinghu formation in Pinghu Slope, Xihu Sag, East China Sea Basin. Journal of Jilin University (Earth Science Edition) 54, 1494–1505 (in Chinese with English abstract). 10.13278/j.cnki.jjuese.20230183.
He, X., Jiang, Y., Li, L., Zhong, R., Feng, Z., Zhang, W., 2024. Progressive deformation characteristics and mechanism of Longjing movement in Xihu Sag. China Offshore Oil and Gas 36, 34–43 (in Chinese with English abstract).
Hu, C., Han, C., Ma, J., Wang, W., Zhao, F., Sun, W., 2023. Reconstruction of paleowind directions during the Cambrian-Ordovician in the Tarim Basin, Northwestern China. Palaeogeography, Palaeoclimatology, Palaeoecology 609, 111316. https://doi.org/10.1016/j.palaeo.2022.111316.
Hu, X., Fang, G., Ge, Y., 2024. Simplified models of wind-wave relationships in China's shallow-water coasts based on SWAN+ADCIRC simulations. Ocean Engineering 305, 117983. https://doi.org/10.1016/j.oceaneng.2024.117983.
Jiang, Z., Deng, H., Lin, H., Wang, L., 2009. Methods and application of paleo-geomorphologies rebuilding: an example of the second member of Shahejie Formation, Zhuangxi Area, Jiyang Depression. Geoscience 23, 865–871 (in Chinese with English abstract).
Jiang, Z., Liu, H., Zhang, S., Su, X., Jiang, Z., 2011. Sedimentary characteristics of large-scale lacustrine beach-bars and their formation in the Eocene Boxing Sag of Bohai Bay Basin, East China. Sedimentology 58, 1087–1112. https://doi.org/10.1111/j.1365-3091.2010.01196.x.
Jiang, Z., Wang, J., Zhang, Y., 2015. Advances in beach-bar research: a review. Journal of Palaeogeography (Chinese Edition) 17, 427–440 (in Chinese with English abstract).
Jiang, Z., Wang, J., Fulthorpe, C.S., Liu, L., Zhang, Y., Liu, H., 2018. A quantitative model of paleowind reconstruction using subsurface lacustrine longshore bar deposits – an attempt. Sedimentary Geology 371, 1–15. https://doi.org/10.1016/j.sedgeo.2018.04.004.
Jiang, Z., Wang, J., Zhang, Y., Zhang, J., Song, M., Wang, Y., Jiang, H., 2020. Ternary "Windfield-Source-Basin" system for the prediction of hydrocarbon reservoirs: interpretation and prediction of hydrocarbon reservoirs deviated from the main provenance areas. Acta Petrolei Sinica 41, 1465–1476 (in Chinese with English abstract).
Keulegan, G.H., 1948. An Experimental Study of Submarine Sand Bars. Technical Report, No. 3. Beach Erosion Board. Office of the Chief of Engineers, Corps of Engineers, U.S. Army.
Kifumbi, C., Scherer, C.M.D.S., Michel, R.D.L., Reis, A.D.D., Guadagnin, F., Souza, E.G.D., Ferronatto, J.P.F., Jones, F.H., 2023. Spatial and temporal variation in the evolution of ancient aeolian dune-field. The Pennsylvanian Piauí Formation (Parnaíba Basin), Brazil. Sedimentary Geology 451, 106398. https://doi.org/10.1016/j.sedgeo.2023.106398.
Lagroix, F., Banerjee, S.K., 2002. Paleowind directions from the magnetic fabric of loess proϕles in central Alaska. Earth and Planetary Science Letters 195, 99–112.
Le Roux, J.P., 2007a. A function to determine wavelength from deep into shallow water based on the length of the cnoidal wave at breaking. Coastal Engineering 54, 770–774. https://doi.org/10.1016/j.coastaleng.2007.05.004.
Le Roux, J.P., 2007b. A simple method to determine breaker height and depth for different deepwater wave height/length ratios and sea floor slopes. Coastal Engineering 54, 271–277. https://doi.org/10.1016/j.coastaleng.2006.10.001.
Le Roux, J.P., 2015. Entrainment threshold of sand- to granule-sized sediments under waves. Sedimentary Geology 322, 63–66. https://doi.org/10.1016/j.sedgeo.2015.04.002.
Le Roux, J., Demirbilek, Z., Brodalka, M., Flemming, B., 2010. WAVECALC: an Excel-VBA spreadsheet to model the characteristics of fully developed waves and their influence on bottom sediments in different water depths. Geo-Marine Letters 30, 549–560. https://doi.org/10.1007/s00367-010-0195-x.
Li, S., Shao, L., Liu, J., Qin, L., Kang, S., Eriksson, K.A., Chen, X., Yu, Z., Liu, J., 2022. Oil generation model of the liptinite-rich coals: Palaeogene in the Xihu Sag, East China Sea Shelf Basin. Journal of Petroleum Science and Engineering 209, 109844. https://doi.org/10.1016/j.petrol.2021.109844.
Li, Y., Zhang, C., Zhao, S., Qi, H., Cai, F., Zheng, J., 2024a. Equilibrium configurations of sandy-muddy transitional beaches on South China coasts: role of waves in formation of sand-mud transition boundary. Coastal Engineering 187, 104401. https://doi.org/10.1016/j.coastaleng.2023.104401.
Li, S., Yu, W., Qin, L., Zhang, C., 2024b. Sand-controlling model of source–slope-break coupling in Pinghu Slope Belt, Xihu Sag. Marine Geology Frontiers 40, 36–44 in Chinese with English abstract. 10.16028/j.1009-2722.2023.119.
Liu, Y., 2020. Response to astronomical forcing of sedimentary record in Xihu Depression, East China Sea Basin. Bulletin of Geological Science and Technology 39, 120–128 in Chinese with English abstract. 10.19509/j.cnki.dzkq.2020.0313.
Liu, B., Zhao, Y., Liang, A., Sun, A., Zhang, Z., Ge, J., Zhao, H., Chen, F., 2024. Quantitative contributions of different atmospheric circulation systems to Holocene aeolian activity in northwestern China: evidence from a closed interdune lake in the Tengger Desert hinterland. Global and Planetary Change 243, 104621. https://doi.org/10.1016/j.gloplacha.2024.104621.
Mau, M., Bjerrum, C.J., Clemmensen, L.B., 2022. Late Triassic paleowinds from lacustrine wave ripple marks in the Fleming Fjord Group, central East Greenland. Palaeogeography, Palaeoclimatology, Palaeoecology 586, 110776. https://doi.org/10.1016/j.palaeo.2021.110776.
Miller, K.G., Browning, J.V., Schmelz, W.J., Kopp, R.E., Mountain, G.S., Wright, J.D., 2020. Cenozoic sea-level and cryospheric evolution from deep-sea geochemical and continental margin records. Science Advances 6, eaaz1346.
Moore, L.J., Sullivan, C., Aubrey, D.G., 2003. Interannual evolution of multiple longshore sand bars in a mesotidal environment, Truro, Massachusetts, USA. Marine Geology 196, 127–144. https://doi.org/10.1016/S0025-3227(03)00028-8.
Pruszak, Z., RóŻyński, G., Zeidler, R.B., 1997. Statistical properties of multiple bars. Coastal Engineering 31, 263–280. https://doi.org/10.1016/S0378-3839(97)00010-0.
Ruessink, B.G., Kroon, A., 1994. The behaviour of a multiple bar system in the nearshore zone of Terschelling, the Netherlands: 1965–1993. Marine Geology 121, 187–197. https://doi.org/10.1016/0025-3227(94)90030-2.
Sakai, T., Battjes, J.A., 1980. Wave shoaling calculated from Cokelet's theory. Coastal Engineering 4, 65–84. https://doi.org/10.1016/0378-3839(80)90006-X.
Su, A., Chen, H., Lei, M., Li, Q., Wang, C., 2019. Paleo-pressure evolution and its origin in the Pinghu slope belt of the Xihu Depression, East China Sea Basin. Marine and Petroleum Geology 107, 198–213. https://doi.org/10.1016/j.marpetgeo.2019.05.017.
Taylor, A.W., Ritts, B.D., 2004. Mesoscale heterogeneity of fluvial-lacustrine reservoir analogues: examples from the Eocene Green River and Colton Formations, Uinta Basin, Utah, Usa. Journal of Petroleum Geology 27, 3–26. https://doi.org/10.1111/j.1747-5457.2004.tb00042.x.
Thornton, E.B., Humiston, R.T., Birkemeier, W., 1996. Bar/trough generation on a natural beach. Journal of Geophysical Research: Oceans 101, 12097–12110. https://doi.org/10.1029/96JC00209.
Troiani, B.T., Simms, A.R., Dellapenna, T., Piper, E., Yokoyama, Y., 2011. The importance of sea-level and climate change, including changing wind energy, on the evolution of a coastal estuary: Copano Bay, Texas. Marine Geology 280, 1–19. https://doi.org/10.1016/j.margeo.2010.10.003.
Wang, J., 2016. Sedimentary Dynamics of a Wind-Source-Basin System in the Eocene Dongying Depression. China University of Geosciences, Beijing (in Chinese with English abstract).
Wang, J., Muto, T., 2021. Autostratigraphic modelling of the growth of alluvial-shelf systems during steady base-level cycles: two-dimensional tank experiments. Sedimentology 68, 135–167. https://doi.org/10.1111/sed.12789.
Wang, Y., Zou, Z., 2016. Longshore currents over barred beach with mild slope. China Ocean Engineering 30, 193–204. https://doi.org/10.1007/s13344-016-0011-0.
Wang, J., Jiang, Z., Xian, B., Zhang, C., Liu, L., 2018a. Advances in paleowind strength reconstruction techniques: use of transporting capacity analysis. Earth Science Frontiers 25, 309–318 (in Chinese with English abstract). 10.13745/j.esf.yx.2017-12-26.
Wang, J., Jiang, Z., Xian, B., Chen, J., Wang, X., Xu, W., Liu, H., 2018b. A method to define the palaeowind strength from lacustrine parameters. Sedimentology 65, 461–491. https://doi.org/10.1111/sed.12388.

Wang, J., Jiang, Z., Xian, B., Zhang, C., Li, G., 2021. Determination of palaeowind strength by using scale of beach-bar sand bodies. Journal of Palaeogeography (Chinese Edition) 23, 937–950 (in Chinese with English abstract).
Wang, T., He, C., Hu, H., Zhang, T., Tang, Y., Diao, H., He, J., 2024. Crude oil source in the western slope zone of Xihu sag. China Offshore Oil and Gas 36, 37–48 (in Chinese with English abstract).
Wu, F., Ren, P., Tan, M., Zhang, F., Ma, H., 2022. Facies evolution and its controlling factors of the Pinghu Formation in the Kongqueting area of Xihu Depression, the East China Sea. Marine Geology & Quaternary Geology 42, 119–130 (in Chinese with English abstract). 10.16562/j.cnki.0256-1492.2021052401.
Xie, H., Liu, C., Zhang, H., Zhang, Z., Xu, H., Wei, X., 2024. Reconstruction of paleowind direction in the Qinghai Lake area during the last deglacial: insights from anisotropy of magnetic susceptibility. Palaeogeography, Palaeoclimatology, Palaeoecology 650, 112351. https://doi.org/10.1016/j.palaeo.2024.112351.
Xu, D., Qin, L., Li, J., Cai, K., Xie, J., 2024. Sequence stratigraphic architectures and sand-body distribution models of the Pinghu Formation in the Pingbei slope belt of the Xihu Depression. Bulletin of Geological Science and Technology 43, 154–166 in Chinese with English abstract. 10.19509/j.cnki.dzkq.tb20240027.
Xue, X., Zhang, Y., Jiang, Z., Wang, L., Wang, S., Jiang, H., 2021. Wave and storm signals in a lacustrine succession and their relationship to paleowind direction (Tanan Depression, Mongolia, early Cretaceous). Sedimentary Geology 419, 105911. https://doi.org/10.1016/j.sedgeo.2021.105911.
Yan, B., Yuan, H., Li, N., Zou, W., Sun, P., Li, M., Zhao, Y., Zhao, Q., 2024. Differences in hydrocarbon accumulation and controlling factors of slope belt in graben basin: a case study of Pinghu Slope Belt in the Xihu sag of the east China Sea Shelf basin (ECSSB). Petroleum Science 21, 2901–2926. https://doi.org/10.1016/j.petsci.2024.06.007.
Young, I.R., Ribal, A., 2019. Multiplatform evaluation of global trends in wind speed and wave height. Science 364, 548–552. https://doi.org/10.1126/science.aav9527.
Young, I.R., Zieger, S., Babanin, A.V., 2011. Global trends in wind speed and wave height. Science 332, 451–455. https://doi.org/10.1126/science.1197219.
Zhu, X., 2020. Sedimentology, fifth edition. Petroleum Industry Press, Beijing (in Chinese).